Membrane-Based Two Phase Heat Sinks for High Heat Flux Electronics and Lasers

Suhas Rao Tamvada, Morteza Alipanah, and Saeed Moghaddam

***Abstract*— Thermal management is the current bottleneck in advancement of high-power integrated circuits (ICs), and phase change heat sinks are a promising solution. With a unique structural configuration consisting of a membrane positioned above the heater surface, membrane-based heat sinks (MHSs) have thus far attained heat fluxes of up to 2 kW/cm^2 and heat transfer coefficient (HTC) of up to 1.8 MW/m^2 · K using water as the working fluid. This work reports the latest progress and performance evaluation of MHS for high flux thermal management. MHS is implemented in conjunction with a low surface tension liquid to rapidly expel bubbles from the heated surface and reach a critical heat flux (CHF) of 340 W/cm^2 and a HTC of 120 kW/m^2 · K. A parametric comparison shows that thermal efficiency, defined as the ratio of cooling capacity and pumping power consumption, of the prototypical devices exceeds values reported hitherto in literature by more than two orders of magnitude. Our results indicate that coupled with the surfaces of higher thermal conductivity and membranes of higher permeability, the MHS devices could be a promising solution to thermal management needs of high-power electronics and lasers.**

***Index Terms*— Critical heat flux (CHF), electronics cooling, heat transfer coefficient (HTC), membrane-based heat sink (MHS), microfabrication, thermal management.**

I. Introduction

THE ever-increasing energy density of integrated circuits (ICs) has led to heat fluxes far exceeding the limits of traditional thermal management methods [1]. Many commercial and military applications using GaN power amplifiers and laser diodes are currently limited to a fraction of their power potential due to the lack of an adequate thermal management solution. The operating cost of data centers (DCs) is directly tied to the performance of their cooling systems. Implementation of single-phase liquid convection cooling has been a major technological leap in thermal management of ICs. The phase change process can further push the cooling limits, as it produces extremely high heat transfer coefficients (HTCs), owing to rapid interruption of the thermal boundary layer by bubbles [2] and formation of liquid films as thin as micrometers on the heat transfer surface [3], [4]. The phase change process can increase temperature uniformity across the device and greatly reduce the cooling liquid flow rate.

Despite its potential to significantly surpass the capability of single-phase convection cooling and enable next-generation high power density ICs, the implementation of two-phase heat sinks is lagging, since the current two-phase heat sinks do not offer substantial improvement relative to the single-phase heat sinks. Years of research and development efforts on enhanced surface structures and fluid delivery methods have led to high-performance single-phase heat sinks. Most single-phase heat sinks use water with additives to avoid freezing and enhance longevity, while two-phase water-based heat sinks and systems are prone to freezing [5]. Furthermore, performance of water-based two-phase heat sinks which are often reported at 100 °C drastically declines when operated at subatmospheric pressure necessary to accommodate the silicon junction temperature [6]. Alternative fluids with lower saturation temperatures have a significantly lower critical heat flux (CHF) and HTC relative to water-based heat sinks [7]. Finally, two-phase systems consisting of multiple heat sinks are complex to operate.

A recently invented [8] membrane-based heat sink (MHS) addresses these issues. Fazeli *et al.* [9] and Fazeli and Moghaddam [10] radically enhanced the CHF and HTC through the implementation of this technique. With the help of a small pressure potential in MHS, Alipanah and Moghaddam [11] reported an order of magnitude increase in CHF compared with the existing heat sinks. In this study, we report our most recent progress and advancement in this field relevant to DCs and also provide a comparison of MHS performance with the existing heat sink technologies. Performance of MHS with ethanol as the working fluid is presented to address the high boiling temperature and freezing issues of a water-based system. In all, our attention is focused on assessing three salient characteristics of MHS: 1) CHF; 2) HTC; and 3) thermal efficiency.

A. Working Principle of MHS

An MHS leverages a contrast in surface wettability and a pressure gradient to actively reduce the residence time of bubbles on the heater. Its unique design places it in the intermediary between pool boiling and flow boiling. To understand the operating mechanism of am MHS, it is imperative to look at the working mechanism of the conventional flow boiling heat sinks as depicted in Fig. 1(a). Due to a liquid inlet and two-phase flow outlet, any bubble generated inside the channel

Manuscript received July 1, 2021; revised August 29, 2021; accepted September 20, 2021. Date of publication September 23, 2021; date of current version October 28, 2021. This work was supported by the U.S. National Science Foundation (NSF) under Grant CBET-1934354, with Dr. Ying Sun as the Program Manager. Recommended for publication by Associate Editor M. Iyengar upon evaluation of reviewers' comments. *(Corresponding author: Saeed Moghaddam.)*

The authors are with the Department of Mechanical and Aerospace Engineering, University of Florida, Gainesville, FL 32611 USA (e-mail: saeedmog@ufl.edu).

Color versions of one or more figures in this article are available at https://doi.org/10.1109/TCPMT.2021.3115419.

Digital Object Identifier 10.1109/TCPMT.2021.3115419

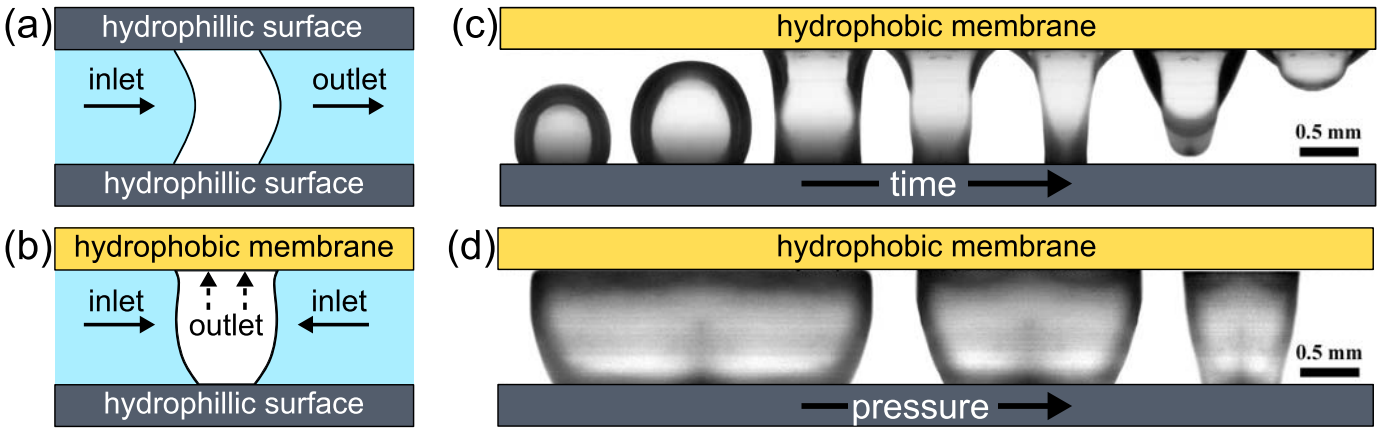

Fig. 1. Working principle of an MHS. (a) Typical two-phase flow in a microchannel with a liquid inlet on one side and a liquid-vapor outlet on the opposite side. (b) MHS without a liquid outlet, forcing the vapor bubble out of the liquid pool constrained between the surface and the vapor-permeable membrane. (c) Bubbles during an adiabatic test performed to illustrate bubble growth and removal through the membrane. A hydrophobic vapor-permeable membrane is used to achieve a contrast in wettability. (d) Effect of pressure on a vapor column-as pressure is increased from 5.7 to 26.4 kPa, the maximum width of the column is decreased.

grows and moves along the channel, displacing the liquid near the heater surface. Such microchannel flow mechanisms rely on thin-film evaporation at the channel walls to remove heat. David *et al.* [12] studied flow boiling in a vapor venting two-phase flow channel and found that 100% bubble removal was not possible; however, they reported a significant decline in pressure drop in the channel. The fundamental issue with all these approaches is that the presence of bubbles in the channels increases, impeding surface rewetting, leading to CHF.

In contrast, an MHS, as illustrated in Fig. 1(b), consists of a millimeter-scale liquid channel, with a hydrophobic vapor-permeable membrane held above a hydrophilic heater surface. The channel has one liquid inlet, and no liquid outlet, with the liquid inside subjected to a positive pressure. A vapor bubble generated on the surface grows until it encounters the membrane, at which point the contact line of the liquid rapidly recedes, ejecting the bubble out of the heat sink. An adiabatic experiment performed to illustrate the working principle of the MHS is shown in Fig. 1(c). A liquid channel consisting of a hydrophilic silicon surface and a hydrophobic nanofibrous PTFE membrane, separated by $\sim$1 mm, is filled with water and pressurized to 7.5 kPa. An air bubble is then introduced through a 5-μm hole in the bottom surface at a constant flow rate of 1.67 mL/min [9]. As the bubble grows and encounters the membrane, the contact line recedes on the membrane subjecting the bubble to a vertical force pulling it away from the hydrophilic surface. This phenomenon in conjunction with a slightly pressurized liquid pool expels the bubble from the channel. The expulsion of the bubble is accompanied by re-wetting of the hydrophilic surface.

While the dynamics of bubble deformation and removal are governed by the interfacial tension of the liquid and vapor, the bubble removal rate is determined by the pressure inside the channel and membrane permeability. A higher pressure in the channel leads to faster bubble removal as shown by Fazeli *et al.* [9]. To study the effect of pressure on bubble size, air was injected through a 400-μm hole at different channel pressures—5.7, 15.1, and 26.4 kPa, as shown in Fig. 1(d). An increase in channel pressure evidently leads to a decrease in bubble size, making this an attractive method to remove bubbles from a heated surface. This mechanism has been leveraged to study boiling characteristics and CHF limits on copper surfaces [9]–[11]. It is important to note that the mechanism discussed above must not be confused with similar work by Lu *et al.* [13] and Hanks *et al.* [14] which use nanoporous membranes for formation and evaporation of thin liquid films.

II. Methodology

As discussed in Section I-A, the key aspects of an MHS are the vapor-permeable hydrophobic membrane and the hydrophilic surface. Hence, studies on MHS have focused on optimization of the membrane and surface to yield the best results. Initially, Fazeli *et al.* [9] used a nanofibrous PTFE membrane to vent out the vapor; however, in a subsequent work, Fazeli and Moghaddam [10] used three different commercial membranes and showed that below a certain channel pressure, the CHF is limited by the permeability of the membrane. To overcome this limitation, Alipanah and Moghaddam [11] developed a custom-made membrane from SU-8 and reported results which corroborated the predictions of Fazeli and Moghaddam [10]. This section provides details on the materials and methods used to study boiling in MHS.

A. Membranes

Two-phase boiling applications commonly use water as the working fluid due to its high latent heat of vaporization (h_{fg}). However, to facilitate boiling and phase change at lower temperatures, especially in applications where junction temperatures range from 60 °C to 80 °C, alternative liquids are commonly used [2]. Ethanol, with a saturation temperature of 78.2 °C at atmospheric pressure (1 atm), is an example of a low surface tension boiling liquid. Accordingly, we restrict our focus to the performance of MHS using water and ethanol.

TABLE I
PORE SIZE AND PERMEABILITY OF MEMBRANES

Membrane material	Avg. Pore size (μm)	Permeability (l/hr-cm^2-kPa)
Polytetrafluoroethylene (PTFE) [10]	15	0.7
SU-8 + metal mesh [11]	10	5.8
Oleophobic ePTFE (present work)	5	4.6

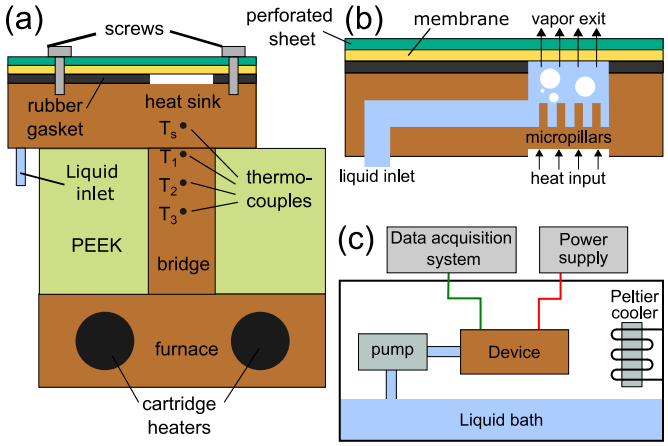

Fig. 2. (a) Test setup consists of three components: 1) MHS housing the test surface; 2) bridge region which transports heat to the surface; and 3) furnace which houses cartridge heaters to generate heat. The bridge section is insulated using PEEK to minimize heat losses. (b) MHS consists of a liquid inlet to the test surface and a vapor outlet via the membrane. Micropillars are machined on the test surface using a micro CNC. (c) Experiments are conducted in a vacuum chamber at atmospheric pressure, and a piezoelectric micropump is used to control liquid pressure and flow rate. A pressure transducer is used to record channel pressure, and a DAQ records temperature and pressure at an interval of 5 s. A Peltier cooler on the chamber wall is used to condense vapor.

While previous generations of MHS have used nanofibrous PTFE membranes and custom-made SU-8 membranes to reach higher heat fluxes with water, they are not oleophobic and thus cannot restrict the entry of lower surface tension liquids into the membrane. For the current tests using ethanol, an oleophobic ePTFE membrane (Parker Performance Materials, Lee's Summit, MO, USA) with an average pore size of 5 μm and a permeability of 4.6 L/hr $\cdot$ cm^2 $\cdot$ kPa is used. Table I shows the details of membranes used in different generations of MHS.

B. Fabrication of Heat Sinks

A cross-sectional view of the MHS fabricated using 101 copper ($k = 394$ W/m $\cdot$ K) on a micro-CNC machine is shown in Fig. 2(b). The effect of heat transfer area and surface wickability on CHF for water has been investigated by Fazeli and Moghaddam [10], and it was reported that an enhanced area ratio (A_r) of 3.45 gave the best results among all tested surfaces. A_r is defined as the ratio of the actual surface area to the projected area of the surface and is given in the following equation:

$$A_r = 1 + \frac{4wh}{(s+w)^2}. \tag{1}$$

Therefore, an array of micropillars are machined on the heat sinks to obtain a surface with pillar height $h = 500$ μm, width $w = 150$ μm, and spacing $s = 200$ μm between the pillars, resulting in a surface with $A_r = 3.45$. The device has an entry channel of cross-sectional area 1×1 mm^2 which supplies liquid to the test section with an effective heated area of 7×7 mm^2. The inlet channel is coated with a 200-μm-thick thermally insulating epoxy to ensure that the test liquid does not boil in the channel [11], [15]. This is achieved by initially machining a channel of cross-sectional area 1.2×1.4 mm^2, filling the channel with epoxy, and re-machining to a cross section of 1.0×1.0 mm^2. To maximize the wetting of the working liquid on the test surface, an oxide layer <1 μm thick is thermally grown on the test surface, resulting in an ethanol contact angle of $\approx 4°$. The membrane is affixed to the heat sink with the help of a perforated metal sheet as shown in Fig. 2(a) and (b). An insulating rubber gasket of thickness 200 μm functions as a spacer between the membrane and the heat sink, resulting in an effective distance of 1.2 mm between the test surface and the membrane.

The wickability (Wi) of structured surfaces, qualitatively described as the ability of surfaces to allow capillary wicking of liquids, is known to increase the CHF during boiling [16]. Surface wickability has been quantified using multiple approaches, most commonly using Darcy's law [17], where the mass flux of the liquid is estimated using the permeability of the structure and the capillary pressure of the liquid. For the purpose of this study, the surface wickability is defined as the product of permeability (K_{wick}) and capillary pressure (P_c), eliminating the use of any *ad hoc* parameters. The permeability and capillary pressure are calculated using the existing models which have been experimentally verified [18], [19], and the wickability of the surface (with $A_r = 3.45$) used in the present study is 0.757 Pa/m^2.

C. Experimental Setup

The test setup consists of an apparatus previously described in detail by Alipanah and Moghaddam [11] and is shown in Fig. 2(c). The device comprises three components: a furnace region which is connected to a bridge region, which supplies heat to the MHS [see Fig. 2(a)]. The furnace region houses two cartridge heaters of 300 W each. Three "k"-type thermocouples spot welded using 28-Gauge wires are embedded into 0.7-mm-diameter holes in the bridge section to measure temperature. The holes, separated by a distance of 4 mm from each other, are greased with a thermal paste to minimize the thermal resistance between the bridge section and the thermocouple junction. The heat flux through the surface is calculated using a three-point backward difference Taylor's approximation as given in the following equation:

$$q'' = k \times \frac{3T_3 - 4T_2 + T_1}{2\Delta x} \tag{2}$$

where k is the thermal conductivity of copper, T_1, T_2, and T_3 are the temperatures recorded by the thermocouples as shown in Fig. 2(a), and Δx is the distance between two consecutive thermocouples (4 mm). A fourth thermocouple (T_s) on the heat sink measures the surface temperature. The bridge section is further enclosed in an insulation of polyether ether ketone

(PEEK) ($k = 0.29$ W/m · K) to minimize heat loss to the surroundings.

The experiments are conducted in a custom-made vacuum chamber at atmospheric pressure to maintain consistent ambient conditions, and a schematic of the test setup is shown in Fig. 2(c). During the experiment, the heat flux is supplied to the cartridge heaters using an ac power supply and is increased in increments of 10 W/cm^2 till CHF is reached. The working liquid is pumped into the MHS using a piezoelectric micropump (Bartels Mikrotechnik GmbH, Model MP6) capable of independently controlling the liquid pressure and flow rate by tuning the voltage and frequency. A pressure transducer (Omega PX26) monitors the pressure inside the heat sink, while an Agilent data acquisition system (DAQ) is used to record the temperature and pressure data at an interval of 5 s. The vapor generated from the device is condensed on the walls of the chambers using a Peltier cooler. Each test was conducted three times to ensure repeatability.

D. Error Analysis

The uncertainty in calculating the heat flux arises from the temperature (ΔT), thermal conductivity of copper (k), and spacing between the thermocouples (Δx). The uncertainty in heat flux is thus given by the following equation:

$$\frac{\delta q''}{q''} = \left[\left(\frac{\delta k}{k}\right)^2 + \left(\frac{\delta \Delta T}{\Delta T}\right)^2 + \left(\frac{\delta \Delta x}{\Delta x}\right)^2\right]^{1/2} \tag{3}$$

where δk, $\delta \Delta T$, and $\delta \Delta x$ are the uncertainties in thermal conductivity, temperature gradient, and spacing, respectively. Since we know that $\Delta T = 3T_3 - 4T_2 + T_1$, $\delta \Delta T$ is calculated as $\delta \Delta T = [(3\delta T)^2 + (4\delta T)^2 + (\delta T)^2]^{1/2} \sim 5.09\delta T$. The uncertainty in HTC in calculated using the following equation:

$$\frac{\delta h}{h} = \left[\left(\frac{\delta q}{q}\right)^2 + \left(\frac{\delta \Delta T_{\text{sup}}}{\Delta T_{\text{sup}}}\right)^2 + \left(\frac{\delta A}{A}\right)^2\right]^{1/2} \tag{4}$$

where ΔT_{sup} is the surface superheat and A is the surface area of the heater. The uncertainty in heat flux was 11.6% at its maximum (lower heat fluxes) and the maximum uncertainty in the HTC was 31.4%.

III. Results and Discussion

As described in Section I-A, MHS leverages positive pressure in the channel along with a polarity in wettability between the surface and the membrane to actively extract vapor bubbles from the heater surface. To study salient boiling characteristics of MHS, a series of boiling tests were performed at discrete pool pressures P_p in the channel while the chamber pressure P_v was maintained at atmospheric pressure ($P_v = 101.3$ kPa). As the liquid in the channel reaches its boiling point, heterogeneous nucleation leads to bubble formation and growth on the surface. Bubble growth and removal proceed through the process described in Section I-A owing to the combined effect of membrane hydrophobicity and imposed pressure. Consequently, the surrounding saturated liquid replaces the bubble to protract the boiling process. Furthermore, surface wickability and heat transfer area are enhanced by the presence of microstructures, augmenting liquid replenishment to the surface. We begin our assessment by first comparing the CHF and HTC obtained using ethanol with our previous results using water.

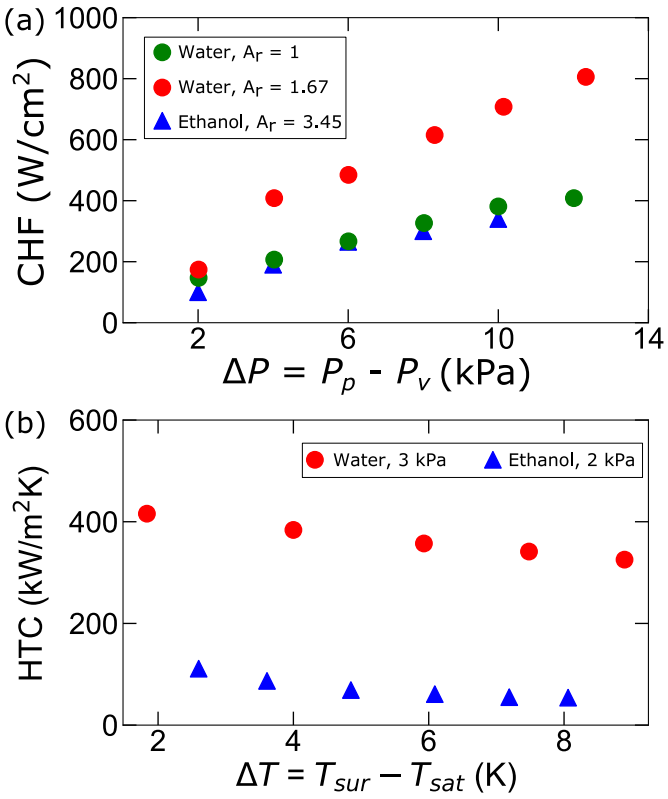

Fig. 3. (a) CHF obtained using ethanol on a surface with $A_r = 3.45$, compared against CHF obtained for water with $A_r = 1$, 1.67. (b) HTCs of ethanol and water at 2 and 3 kPa, respectively, for a surface with $A_r = 3.45$ (see [11]).

A. CHF and HTC of Ethanol

To measure the heat sink's CHF, each test was performed at a distinct channel pressure P_p. A constant heat flux was supplied to the surface till the temperatures reached a plateau and was subsequently increased in incremental steps till a sudden jump in temperatures was observed. The heat flux at this point was noted to be the CHF for the corresponding pressure difference $\Delta P = P_p - P_v$. Fig. 3(a) shows the CHF plotted against device pressure ($\Delta P = P_p - P_v$). The CHF obtained using ethanol with the highest area ratio ($A_r = 3.45$) is comparable to the CHF obtained using water on a plain surface ($A_r = 1$). An increase in CHF with pressure is apparent, confirming the hypothesis that an increase in pressure increases the rate of bubble removal. This indicates that with the use of microstructures and a stable liquid rewetting mechanism, ethanol could potentially be a substitute for water in high flux thermal management. It is also noteworthy that while water boiling heat transfer on a surface with $A_r = 1.67$ is limited by membrane permeability at lower pressures (<4kPa), ethanol boiling heat transfer is solely limited by surface properties.

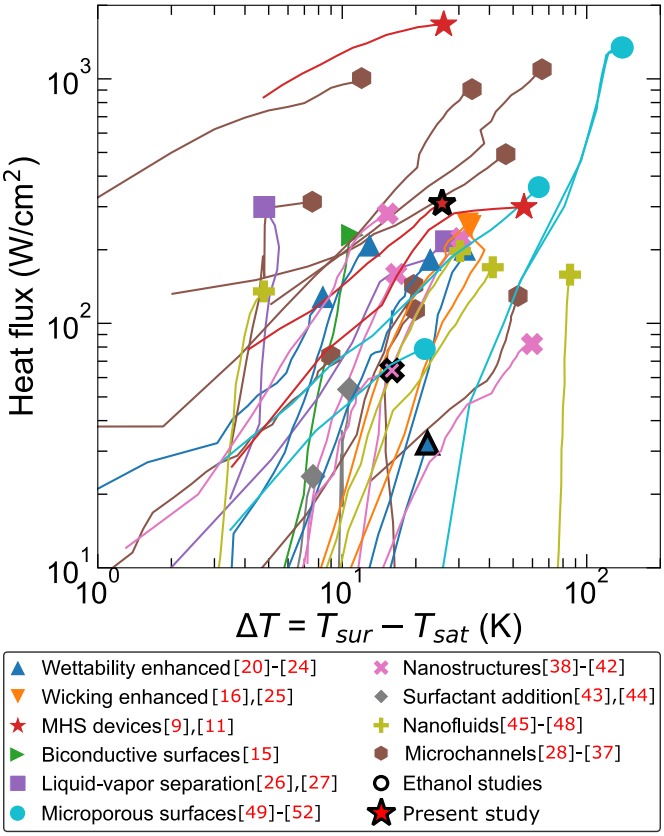

Fig. 4. Comparison of the boiling curves and CHFs of MHS devices and boiling studies reported in literature, as a function of surface superheat ΔT [9], [11], [15], [16], [20]–[52]. The lines represent the boiling curves and the circle markers represent the highest heat flux obtained. The markers with black outline represent studies with ethanol, such as the present study represented by ★.

Furthermore, effectiveness of heat removal is important to applications such as DC cooling due to large thermal loads and resulting costs associated with it [53]. Thus, in addition to higher heat fluxes, many electronics applications benefit greatly from a higher HTC. Fig. 3(b) shows the comparison between HTC of ethanol and water at 2 and 3 kPa, respectively. Both sets of data points are for a surface with $A_r = 3.45$. As expected, HTC is maximum at lower superheats. These results indicate that although heat fluxes comparable to water can be obtained using ethanol, HTCs using ethanol are considerably lower than those of water at similar surface superheat conditions.

B. Comparison of CHF

From an understanding of the differences between boiling performance of ethanol and water, we proceed to assess the performance of MHS with heat sink technologies and boiling enhancement techniques available in the literature. Fig. 4 shows the boiling curves and CHF limits for different generations of MHS along with a representative set of boiling studies in the literature [9], [11], [15], [16], [20]–[52]. The studies using ethanol as the working fluid, such as the present investigation (★), are represented by markers with a black outline.

Numerous strategies have been used to enhance CHF in pool boiling ad flow boiling, such as the use of biphilic and biconductive surfaces [15], [21], [22], functionalized surfaces [23], separated liquid-vapor pathways [26], [27], microchannel flow devices [28]–[37] with sintered surfaces and varying channel cross sections, nanowires and nano-structures [38]–[41], addition of surfactants and nanoparticles [42]–[48], increasing surface roughness and wickability [16], [25], tuning surface wettability [20], and using microporous structures [49]–[52]. Recently, Rahman *et al.* [16] demonstrated through biotemplating of microstructures that an increase in surface roughness and wickability facilitates liquid replenishment to the surface, enhancing CHF. Similarly, surfactant or nanoparticle additives to the working liquid attempt to either lower the surface tension or cause formation of a thin nanoparticle film on the heater surface. Other methods, such as the ordering of liquid-vapor pathways and use of biconductive or biphilic surfaces, aim to achieve the same underlying objectives: 1) decreasing bubble residence time and 2) increasing liquid supply to the surface. Although a multitude of aforementioned technologies enhance CHF marginally, many do not exceed Zuber's limit [54] for plain surfaces by more than 100%–150%. By comparison, heat fluxes obtained by MHS are higher than Zuber's limit (≈130 W/cm^2) by an order of magnitude [$\mathcal{O}(1)$]. The performance of MHS is attributed to the combined effect of increasing surface area, robust rewetting of the surface, and an effective vapor removal mechanism through a pressure potential. The presence of microstructures increases surface wickability while providing an abundance of nucleation sites for bubble inception.

C. Comparison of HTC

Next, we assess the effectiveness of heat transfer through a comparison of HTC as shown in Fig. 5. The HTCs of MHS devices, including the present study, are plotted alongside multiple studies available in the literature [11], [15], [21], [22], [27], [29], [30], [33], [40], [55]. Contrary to its effect on CHF, a surface patterned with hydrophobic and hydrophilic parts promotes an increase in HTC owing to its ability to maximize heat transfer through phase change at lower superheats. Hence, biphilic [21], [22] and biconductive surfaces [15] show a higher HTC compared with other surface enhancements. Separated vapor-liquid pathways also enhance HTC in comparison to enhanced surface structures as shown by Kandlikar [26] and Jaikumar and Kandlikar [34]. An MHS maximizes heat transfer through phase change by continually rewetting the heater surface, resulting in a comparatively higher HTC (see Fig. 5). Investigations under the DARPA ICECool program led by Prof. Avram Bar-Cohen divulged that the pressure drop across the evaporator in high heat flux applications is a predominant contributor to the overall pressure drop. For example, Drummond *et al.* [35] demonstrated through a hierarchical michochannel manifold that heat fluxes of up to 910 W/cm^2 can be removed. However, the pressure potential required to achieve these heat fluxes is close to 160 kPa. MHS demonstrates a potential solution to address this issue.

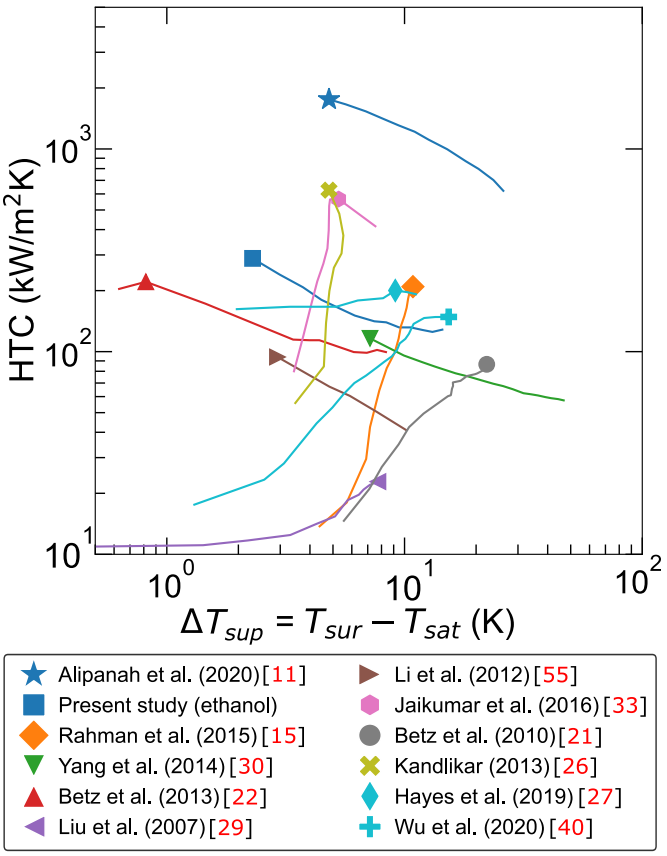

Fig. 5. HTC as a function of surface superheat ΔT_{sup} from various boiling studies available in literature [11], [15], [21], [22], [26], [27], [29], [30], [33], [40], [55].

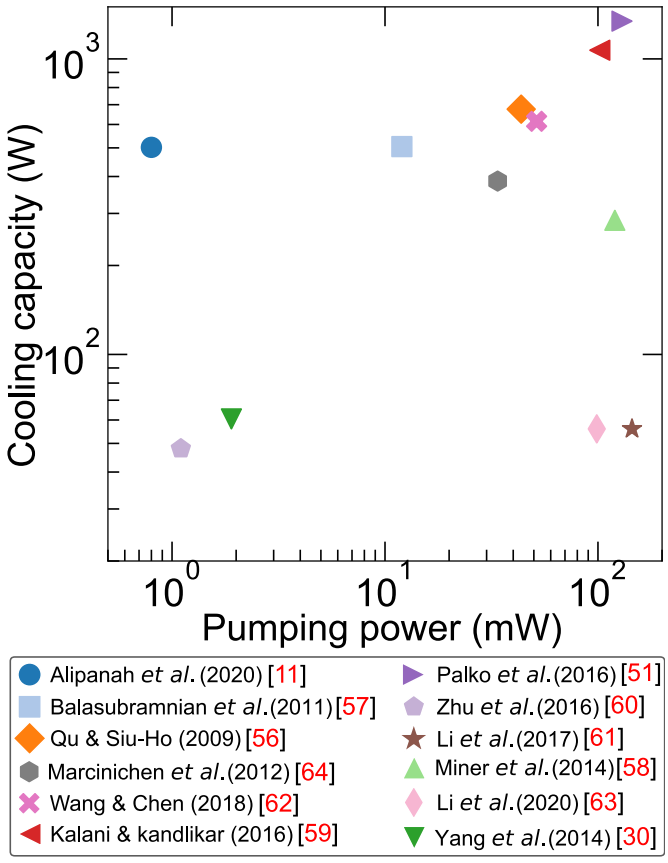

Fig. 6. Comparison of thermal performance of MHS devices with the existing two-phase flow loops [11], [30], [51], [56]–[64]. The maximum cooling capacity is mapped against the required pumping power for each device.

D. Thermal Performance of MHS

In addition to CHF and HTC, thermal efficiency is often used as a metric to characterize different heat sinks, where liquid pumping power may be important. To evaluate the performance of MHS with comparable two-phase heat sinks using an accepted metric, we plot the maximum cooling capacity of various two-phase flow heat sinks against their required pumping power [11], [30], [51], [56]–[64]. While different heat sinks vary in their design to target various needs such as handling high heat loads, or removing high heat fluxes from confined dimensions, for a fair comparison, we choose two-phase flow heat sinks comparable to MHS in their size. An ideal two-phase heat sink must provide a high cooling capacity while using low amount of power. Evidently, MHS satisfies this criterion using close to two orders of magnitude [$\sim\mathcal{O}(2)$] less power than traditional heat sinks as seen in Fig. 6. Membrane-aided bubble removal enables a high vapor quality at the exit and results in an improvement in performance compared with surface modifications alone.

E. Effect of Membrane Permeability on Performance

After assessing the thermal performance of MHS, we now turn our attention to the multiple factors influencing their performance. Fig. 7 illustrates various factors governing the CHF limit in MHS. The solid red line represents typical values of CHF obtained at different pressures. At a lower operating pressure (region I), the maximum vapor flow rate through the membrane (blue strip) inhibits effective vapor

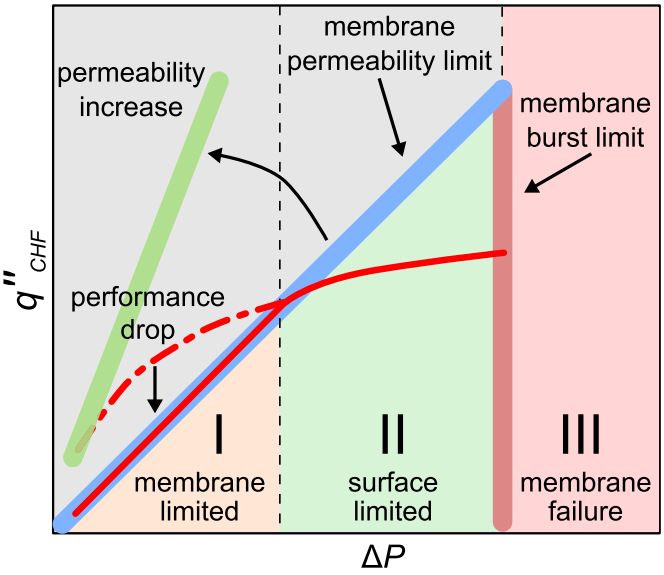

Fig. 7. Phase diagram illustrates factors influencing the performance of MHS. The red line represents typical CHF values across different pressures which are limited by the permeability of the membrane at low pressures (region I) and by surface wickability at moderately higher pressures (region II). Region III represents membrane failure where channel pressures exceed liquid breakthrough pressure of the membrane.

removal from the surface, causing a drop in performance from ideal conditions (red dot dashed line). In this region, CHF is limited by the membrane permeability, and hence increasing membrane permeability leads to an increase in CHF [11]. At moderately higher pressures (region II), mass flow rate through the membrane increases; however, the surface experiences temporary dry spots and ultimately reaches CHF due to lack of liquid supply to the surface. Surface structures have been shown to improve CHF at these pressures (region II) [10]. Finally, liquid breakthrough pressure acts as the upper limit for testing (region III). At these critical pressures, the working liquid penetrates the membrane and testing is stopped. For a given surface, the performance of MHS devices can be improved by increasing the permeability of the membrane while also increasing the liquid breakthrough pressure (maximizing area under regions I and II).

IV. Conclusion

In summary, this work presents a comprehensive analysis of the performance characteristics of MHS technology for high flux thermal management. Our analysis was focused on critical performance metrics relevant to electronics cooling, such as the CHF, HTC, and thermal efficiency of MHS. Details pertinent to the fabrication of heat sinks and testing apparatus are provided. Following boiling studies using ethanol as the working fluid, we report a maximum CHF of 340 W/cm^2 and HTC of 120 kW/m^2 $\cdot$ K. We find through an evaluation of boiling characteristics that MHS provides greater enhancement in CHF compared with surface modifications, conventional microchannels, and particle/surfactant additives to the working fluid. Imposed pressure and constant rewetting of the surface are found to be contributing to significantly higher heat fluxes compared with values reported in the literature. While MHS needs external work input in the form of a positive pressure in the channel, we find through a parametric comparison that the thermal performance of MHS is far superior to the existing heat sink technologies.

References

[1] K. P. Bloschock and A. Bar-Cohen, "Advanced thermal management technologies for defense electronics," *Proc. SPIE Defense Transformation Net-Centric Syst.*, vol. 8405, May 2012, Art. no. 84050I.

[2] S. Moghaddam and K. Kiger, "Physical mechanisms of heat transfer during single bubble nucleate boiling of FC-72 under saturation conditions—I. Experimental investigation," *Int. J. Heat Mass Transf.*, vol. 52, nos. 5–6, pp. 1284–1294, Feb. 2009.

[3] M. H. Matin and S. Moghaddam, "Thin liquid films formation and evaporation mechanisms around elongated bubbles in rectangular cross-section microchannels," *Int. J. Heat Mass Transf.*, vol. 163, Dec. 2020, Art. no. 120474.

[4] M. H. Matin and S. Moghaddam, "Mechanism of transition from elongated bubbles to wavy-annular regime in flow boiling through microchannels," *Int. J. Heat Mass Transf.*, vol. 176, Sep. 2021, Art. no. 121464.

[5] G. Moreno, S. Narumanchi, X. Feng, P. Anschel, S. Myers, and P. Keller, "Electric-drive vehicle power electronics thermal management: Current status, challenges, and future directions," *J. Electron. Packag.*, vol. 144, no. 1, Mar. 2022, Art. no. 011004.

[6] S. M. Kwark, M. Amaya, R. Kumar, G. Moreno, and S. M. You, "Effects of pressure, orientation, and heater size on pool boiling of water with nanocoated heaters," *Int. J. Heat Mass Transf.*, vol. 53, nos. 23–24, pp. 5199–5208, Nov. 2010.

[7] W. Wu, H. Bostanci, L. C. Chow, Y. Hong, M. Su, and J. P. Kizito, "Nucleate boiling heat transfer enhancement for water and FC-72 on titanium oxide and silicon oxide surfaces," *Int. J. Heat Mass Transf.*, vol. 53, nos. 9–10, pp. 1773–1777, Apr. 2010.

[8] S. Moghaddam and S. A. Fazeli, "Hierarchical hydrophilic/hydrophobic micro/nanostructures for pushing the limits of critical heat flux," U.S. Patent 10 897 833, Jan. 19, 2021.

[9] A. Fazeli, M. Mortazavi, and S. Moghaddam, "Hierarchical biphilic micro/nanostructures for a new generation phase-change heat sink," *Appl. Thermal Eng.*, vol. 78, pp. 380–386, Mar. 2015.

[10] A. Fazeli and S. Moghaddam, "A new paradigm for understanding and enhancing the critical heat flux (CHF) limit," *Sci. Rep.*, vol. 7, no. 1, pp. 1–11, Dec. 2017.

[11] M. Alipanah and S. Moghaddam, "Ultra-low pressure drop membrane-based heat sink with 1000 W/cm^2 cooling capacity and 100% exit vapor quality," *Int. J. Heat Mass Transf.*, vol. 161, Nov. 2020, Art. no. 120312.

[12] M. P. David, J. Miler, J. E. Steinbrenner, Y. Yang, M. Touzelbaev, and K. E. Goodson, "Hydraulic and thermal characteristics of a vapor venting two-phase microchannel heat exchanger," *Int. J. Heat Mass Transf.*, vol. 54, nos. 25–26, pp. 5504–5516, Dec. 2011.

[13] Z. Lu *et al.*, "Design and modeling of membrane-based evaporative cooling devices for thermal management of high heat fluxes," *IEEE Trans. Compon., Packag., Manuf. Technol.*, vol. 6, no. 7, pp. 1056–1065, Jul. 2016.

[14] D. F. Hanks *et al.*, "Nanoporous membrane device for ultra high heat flux thermal management," *Microsyst. Nanoeng.*, vol. 4, no. 1, pp. 1–10, Dec. 2018.

[15] M. M. Rahman, J. Pollack, and M. McCarthy, "Increasing boiling heat transfer using low conductivity materials," *Sci. Rep.*, vol. 5, no. 1, pp. 1–11, Oct. 2015.

[16] M. M. Rahman, E. Ölçeroglu, and M. McCarthy, "Role of wickability on the critical heat flux of structured superhydrophilic surfaces," *Langmuir*, vol. 30, no. 37, pp. 11225–11234, 2014.

[17] N. S. Dhillon, J. Buongiorno, and K. K. Varanasi, "Critical heat flux maxima during boiling crisis on textured surfaces," *Nature Commun.*, vol. 6, no. 1, pp. 1–11, Nov. 2015.

[18] A. Tamayol and M. Bahrami, "Transverse permeability of fibrous porous media," *Phys. Rev. E, Stat. Phys. Plasmas Fluids Relat. Interdiscip. Top.*, vol. 83, no. 4, p. 46314, Apr. 2011.

[19] S. Ravi, D. Horner, and S. Moghaddam, "A novel method for characterization of liquid transport through micro-wicking arrays," *Microfluidics Nanofluidics*, vol. 17, no. 2, pp. 349–357, Aug. 2014.

[20] C. H. Wang and V. K. Dhir, "Effect of surface wettability on active nucleation site density during pool boiling of water on a vertical surface," *J. Heat Transf.*, vol. 115, no. 3, pp. 659–669, Aug. 1993.

[21] A. R. Betz, J. Xu, H. Qiu, and D. Attinger, "Do surfaces with mixed hydrophilic and hydrophobic areas enhance pool boiling?" *Appl. Phys. Lett.*, vol. 97, no. 14, Oct. 2010, Art. no. 141909.

[22] A. R. Betz, J. Jenkins, C.-J. Kim, and D. Attinger, "Boiling heat transfer on superhydrophilic, superhydrophobic, and superbiphilic surfaces," *Int. J. Heat Mass Transf.*, vol. 57, no. 2, pp. 733–741, Feb. 2013.

[23] X. Dai *et al.*, "Enhanced nucleate boiling on horizontal hydrophobic-hydrophilic carbon nanotube coatings," *Appl. Phys. Lett.*, vol. 102, no. 16, Apr. 2013, Art. no. 161605.

[24] B. Shen *et al.*, "Enhanced pool boiling of ethanol on wettability-patterned surfaces," *Appl. Thermal Eng.*, vol. 149, pp. 325–331, Feb. 2019.

[25] K.-H. Chu, Y. S. Joung, R. Enright, C. R. Buie, and E. N. Wang, "Hierarchically structured surfaces for boiling critical heat flux enhancement," *Appl. Phys. Lett.*, vol. 102, no. 15, Apr. 2013, Art. no. 151602.

[26] S. G. Kandlikar, "Controlling bubble motion over heated surface through evaporation momentum force to enhance pool boiling heat transfer," *Appl. Phys. Lett.*, vol. 102, no. 5, Feb. 2013, Art. no. 051611.

[27] A. Hayes, P. A. Raghupathi, T. S. Emery, and S. G. Kandlikar, "Regulating flow of vapor to enhance pool boiling," *Appl. Thermal Eng.*, vol. 149, pp. 1044–1051, Feb. 2019.

[28] W. Qu and I. Mudawar, "Flow boiling heat transfer in two-phase micro-channel heat sinks—I. Experimental investigation and assessment of correlation methods," *Int. J. Heat Mass Transf.*, vol. 46, no. 15, pp. 2755–2771, Jul. 2003.

[29] D. Liu and S. V. Garimella, "Flow boiling heat transfer in microchannels," *J. Heat Transf.*, vol. 129, no. 10, pp. 1321–1332, Oct. 2007.

[30] F. Yang, X. Dai, Y. Peles, P. Cheng, J. Khan, and C. Li, "Flow boiling phenomena in a single annular flow regime in microchannels (I): Characterization of flow boiling heat transfer," *Int. J. Heat Mass Transf.*, vol. 68, pp. 703–715, Jan. 2014.

[31] A. Kalani and S. G. Kandlikar, "Enhanced pool boiling with ethanol at subatmospheric pressures for electronics cooling," *J. Heat Transf.*, vol. 135, no. 11, Nov. 2013, Art. no. 111002.

[32] D. Cooke and S. G. Kandlikar, "Pool boiling heat transfer and bubble dynamics over plain and enhanced microchannels," in *Proc. ASME 8th Int. Conf. Nanochannels, Microchannels*, Mar. 2010, pp. 163–172.

[33] A. Jaikumar and S. G. Kandlikar, "Ultra-high pool boiling performance and effect of channel width with selectively coated open microchannels," *Int. J. Heat Mass Transf.*, vol. 95, pp. 795–805, Apr. 2016.

[34] A. Jaikumar and S. G. Kandlikar, "Pool boiling enhancement through bubble induced convective liquid flow in feeder microchannels," *Appl. Phys. Lett.*, vol. 108, no. 4, p. 41604, 2016.

[35] K. P. Drummond *et al.*, "A hierarchical manifold microchannel heat sink array for high-heat-flux two-phase cooling of electronics," *Int. J. Heat Mass Transf.*, vol. 117, pp. 319–330, Feb. 2018.

[36] C. Woodcock, C. Ng'oma, M. Sweet, Y. Wang, Y. Peles, and J. Plawsky, "Ultra-high heat flux dissipation with piranha pin fins," *Int. J. Heat Mass Transf.*, vol. 128, pp. 504–515, Jan. 2019.

[37] R. K. Mandel, D. G. Bae, and M. M. Ohadi, "Embedded two-phase cooling of high flux electronics via press-fit and bonded FEEDS coolers," *J. Electron. Packag.*, vol. 140, no. 3, Sep. 2018, Art. no. 031003.

[38] C. Li, Z. Wang, P.-I. Wang, Y. Peles, N. Koratkar, and G. P. Peterson, "Nanostructured copper interfaces for enhanced boiling," *Small*, vol. 4, no. 8, pp. 1084–1088, Aug. 2008.

[39] T. J. Hendricks, S. Krishnan, C. Choi, C.-H. Chang, and B. Paul, "Enhancement of pool-boiling heat transfer using nanostructured surfaces on aluminum and copper," *Int. J. Heat Mass Transf.*, vol. 53, nos. 15–16, pp. 3357–3365, Jul. 2010.

[40] F. Wu, H. Ze, S. Chen, and X. Gao, "High-efficiency boiling heat transfer interfaces composed of electroplated copper nanocone cores and low-thermal-conductivity nickel nanocone coverings," *ACS Appl. Mater. Interfaces*, vol. 12, no. 35, pp. 39902–39909, Sep. 2020.

[41] R. Chen, M.-C. Lu, V. Srinivasan, Z. Wang, H. H. Cho, and A. Majumdar, "Nanowires for enhanced boiling heat transfer," *Nano Lett.*, vol. 9, no. 2, pp. 548–553, 2009.

[42] L. Dong, X. Quan, and P. Cheng, "An experimental investigation of enhanced pool boiling heat transfer from surfaces with micro/nano-structures," *Int. J. Heat Mass Transf.*, vol. 71, pp. 189–196, Apr. 2014.

[43] J. Zhang and R. M. Manglik, "Additive adsorption and interfacial characteristics of nucleate pool boiling in aqueous surfactant solutions," *J. Heat Transf.*, vol. 127, no. 7, pp. 684–691, Jul. 2005.

[44] H. J. Cho, J. P. Mizerak, and E. N. Wang, "Turning bubbles on and off during boiling using charged surfactants," *Nature Commun.*, vol. 6, no. 1, pp. 1–7, Oct. 2015.

[45] S. M. You, J. H. Kim, and K. H. Kim, "Effect of nanoparticles on critical heat flux of water in pool boiling heat transfer," *Appl. Phys. Lett.*, vol. 83, no. 16, pp. 3374–3376, Oct. 2003.

[46] S. J. Kim, I. C. Bang, J. Buongiorno, and L. W. Hu, "Surface wettability change during pool boiling of nanofluids and its effect on critical heat flux," *Int. J. Heat Mass Transf.*, vol. 50, nos. 19–20, pp. 4105–4116, Sep. 2007.

[47] Z.-H. Liu and L. Liao, "Sorption and agglutination phenomenon of nanofluids on a plain heating surface during pool boiling," *Int. J. Heat Mass Transf.*, vol. 51, nos. 9–10, pp. 2593–2602, May 2008.

[48] S. M. Kwark, R. Kumar, G. Moreno, J. Yoo, and S. M. You, "Pool boiling characteristics of low concentration nanofluids," *Int. J. Heat Mass Transf.*, vol. 53, nos. 5–6, pp. 972–981, Feb. 2010.

[49] S. G. Liter and M. Kaviany, "Pool-boiling CHF enhancement by modulated porous-layer coating: Theory and experiment," *Int. J. Heat Mass Transf.*, vol. 44, no. 22, pp. 4287–4311, Nov. 2001.

[50] C. Li and G. P. Peterson, "Parametric study of pool boiling on horizontal highly conductive microporous coated surfaces," *J. Heat Transf.*, vol. 129, no. 11, pp. 1465–1475, Nov. 2007.

[51] J. W. Palko *et al.*, "High heat flux two-phase cooling of electronics with integrated diamond/porous copper heat sinks and microfluidic coolant supply," in *Proc. 15th IEEE Intersoc. Conf. Thermal Thermomech. Phenomena Electron. Syst. (ITherm)*, May 2016, pp. 1511–1517.

[52] J. W. Palko *et al.*, "Extreme two-phase cooling from laser-etched diamond and conformal, template-fabricated microporous copper," *Adv. Funct. Mater.*, vol. 27, no. 45, Dec. 2017, Art. no. 1703265.

[53] M. K. Patterson, "The effect of data center temperature on energy efficiency," in *Proc. 11th Intersoc. Conf. Thermal Thermomech. Phenomena Electron. Syst.*, May 2008, pp. 1167–1174.

[54] N. Zuber, "Hydrodynamic aspects of boiling heat transfer (thesis)," Ramo-Woolridge Corp., Univ. California, Los Angeles, Los Angeles, CA, USA, Tech. Rep. AECU-4439, 1959.

[55] D. Li *et al.*, "Enhancing flow boiling heat transfer in microchannels for thermal management with monolithically-integrated silicon nanowires," *Nano Lett.*, vol. 12, no. 7, pp. 3385–3390, Jul. 2012.

[56] W. Qu and A. Siu-Ho, "Experimental study of saturated flow boiling heat transfer in an array of staggered micro-pin-fins," *Int. J. Heat Mass Transf.*, vol. 52, nos. 7–8, pp. 1853–1863, Mar. 2009.

[57] K. Balasubramanian, P. S. Lee, L. W. Jin, S. K. Chou, C. J. Teo, and S. Gao, "Experimental investigations of flow boiling heat transfer and pressure drop in straight and expanding microchannels—A comparative study," *Int. J. Thermal Sci.*, vol. 50, no. 12, pp. 2413–2421, 2011.

[58] M. J. Miner, P. E. Phelan, B. A. Odom, and C. A. Ortiz, "Experimental measurements of critical heat flux in expanding microchannel arrays," *J. Heat Transf.*, vol. 135, no. 10, Oct. 2013, Art. no. 101501.

[59] A. Kalani and S. G. Kandlikar, "Evaluation of pressure drop performance during enhanced flow boiling in open microchannels with tapered manifolds," *J. Heat Transf.*, vol. 136, no. 5, May 2014, Art. no. 051502.

[60] Y. Zhu *et al.*, "Surface structure enhanced microchannel flow boiling," *J. Heat Transf.*, vol. 138, no. 9, Sep. 2016, Art. no. 091501.

[61] W. Li *et al.*, "Enhanced flow boiling in microchannels through integrating multiple micro-nozzles and reentry microcavities," *Appl. Phys. Lett.*, vol. 110, no. 1, Jan. 2017, Art. no. 014104.

[62] Q. Wang and R. Chen, "Ultrahigh flux thin film boiling heat transfer through nanoporous membranes," *Nano Lett.*, vol. 18, no. 5, pp. 3096–3103, May 2018.

[63] Y. F. Li, G. D. Xia, D. D. Ma, J. L. Yang, and W. Li, "Experimental investigation of flow boiling characteristics in microchannel with triangular cavities and rectangular fins," *Int. J. Heat Mass Transf.*, vol. 148, Feb. 2020, Art. no. 119036.

[64] J. B. Marcinichen, J. A. Olivier, and J. R. Thome, "On-chip two-phase cooling of datacenters: Cooling system and energy recovery evaluation," *Appl. Thermal Eng.*, vol. 41, pp. 36–51, Aug. 2012.

Suhas Rao Tamvada received the B.Tech. degree from Jawaharlal Nehru Technological University, Hyderabad, India, in 2017, and the M.S. degree from the University of Illinois at Chicago, Chicago, IL, USA, in 2020, all in mechanical engineering. He is currently pursuing the Ph.D. degree in mechanical engineering with the Nanostructured Energy Systems Laboratories, University of Florida, Gainesville, FL, USA, with a focus on critical heat flux enhancement through surface engineering.

Morteza Alipanah received the B.S. degree from Urmia University, Urmia, Iran, in 2007, the M.S. degree from Babol Noshirvani University of Technology, Babol, Iran, in 2009, and the Ph.D. degree from the University of Florida, Gainesville, FL, USA, in 2020, all in mechanical engineering. His research during the Ph.D. degree was focused on experimental investigation of critical heat flux using membrane-based heat sinks.

He is currently a Post-Doctoral Researcher with the Nanostructured Energy Systems Laboratories, University of Florida.

Saeed Moghaddam received the Ph.D. degree in mechanical engineering from the University of Maryland, College Park, MD, USA, in 2006.

He was a Post-Doctoral Researcher with the Chemical and Biomolecular Engineering Department, University of Illinois at Urbana–Champaign, Champaign, IL, USA, from 2007 to 2010. He currently serves as the William F. Powers Professor of the University of Florida, Gainesville, FL, USA, where his research is focused on micro/nanoscale transport and nanotechnology.

Dr. Moghaddam is a fellow of American Society of Mechanical Engineers (ASME).